Spectrochimica Acta Part A: Molecular and Biomolecular Spectroscopy 183 (2017) 371–377

Contents lists available at ScienceDirect

Spectrochimica Acta Part A: Molecular and Biomolecular Spectroscopy

journal homepage: www.elsevier.com/locate/saa

# TDDFT study on recognition mechanism for the oxygen sensing of the cyclometalated platinum (II) complex

Tong Huan [a,b], Zhao Zhengyan [a], Li Guanglan [a], Gao Liguo [a], Zhao Ningjiu [b], Li Peng [b,*], Jia Yan [b], Zhou Chenyang [c], Zhang Mingzhen [c,*], Wang Yong [c], Hao Ce [a,*], Tang Xiaoying [c]

[a] State Key Laboratory of Fine Chemicals, Dalian University of Technology, Panjin 124221, China
[b] State Key Laboratory of Molecular Reaction Dynamics, Dalian Institute of Chemical Physics, Chinese Academy of Sciences, Dalian 116023, China
[c] Tianjin Key Laboratory of Molecular Optoelectronic Sciences, Institute of Chemistry, Department of Chemistry, School of Science, Tianjin University, Tianjin 300354, China

ARTICLE INFO

*Article history:*
Received 13 January 2017
Received in revised form 7 April 2017
Accepted 18 April 2017
Available online 19 April 2017

*Keywords:*
Recognition mechanism
Sensor
Charge transfer
Excited state
H-bond

ABSTRACT

The influence of oxygen molecule on the luminescent properties of a cyclometalated Pt(II) complex Lxp1, was investigated using density functional theory (DFT) and time-dependent density functional theory (TDDFT) methods. Analysis of frontier molecular orbitals and electronic configuration indicated that the highest-occupied molecular orbital of the Lxp1 has a significant mixture of metal Pt (d) as well as 2-phenylpyridine and acetyl acetone($\pi$). The lowest-unoccupied orbital of the Lxp1 primarily locates on $\pi^*$ of 2-phenylpyridineligands. The emission mechanism of the cyclometalated Pt(II) complex Lxp1 is assigned to the mixing of ligand-to-metal charge transfer and ligand-to-ligand charge transfer. The emission mechanism of the Lxp1–$O_2$ complex can be attributed to the charge transfer from the oxygen molecule to the luminescent material Lxp1. Our study showed that intermolecular hydrogen bonding between the Lxp1 and oxygen molecule was strengthened by the calculation of electronic excitation, leading to a luminescence-decreasing phenomenon. The calculation of the radiative and non-radiative decay rate constants of the Lxp1 and the Lxp1–$O_2$ complex demonstrates that the phosphorescence from $T_1$-$S_0$ of the Lxp1 would alter to the internal conversion from $T_1$-$T_0$ of the Lxp1–$O_2$ complex. This alteration further explains the luminescence quenching phenomenon of the cyclometalated Pt(II) complex Lxp1 after interacting with oxygen molecule.



## 1. Introduction

Molecular oxygen, an important Earth component, plays an essential role in various processes, including physiological transformation, chemical and biochemical reactions, and manufacturing protocols [1]. Thus, considerable attention has been devoted to the detection of molecular oxygen. Traditional methods of detecting oxygen molecule include titration [2], measurement with Clark electrodes [3], chemiluminescence [4], and thermoluminescence [5]. These techniques have several limitations, such as long response time, oxygen consumption during monitoring, as well as poor selectivity [6–9]. However, detection by optical oxygen sensors has become an increasingly competitive method for oxygen sensing owing to its fast response, excellent sensitivity and selectivity, low cost, as well as minimal analyte consumption. The primary components of oxygen sensors are oxygen-sensitive probes (OSPs). These OSPs include metal-free probes fullerenes, such as $C_{60}$ and $C_{70}$ [10–13], boron-complex dyes [14,15], as well as organometallic complexes of platinum(II) [16–24], palladium(II) [25–27], ruthenium(II) [28], and iridium(III) [29]. Among these complexes, Pt(II) complexes are widely used because of their extremely long lifetime, varying from microseconds to a few milliseconds [30–33] and high-luminescence quantum yield.

Pt(II) complexes were applied in 1991 for the fiber optic oxygen sensor [34] at the first time. Liu et al. [35] synthesized a series of cyclometalated Pt(II) complexes in 2015. All of the cyclometalated Pt(II) complexes exhibited intense phosphorescence emission at room temperature. They evaluated the oxygen sensitivity of several cyclometalated Pt (II) complexes in accordance with the following Stern–Volmer equation:

$$\frac{I_0}{I} = \frac{\tau_0}{\tau} = 1 + k_q \tau_0 \cdot p_{o_2} \quad (1)$$

where, on the basis of the relationship between the luminous intensity or the lifetime of OSPs and oxygen concentration, $k_q$ is the quenching rate constant, $p_{O2}$ is the partial pressure of oxygen, $I$ is the phosphorescence intensity, $\tau$ is the lifetime of an OSP, and $I_0$ and $\tau_0$ are the corresponding values in the absence of oxygen. However, the mechanism

* Corresponding authors.
*E-mail addresses:* pengl@dicp.ac.cn (P. Li), mingzhen.zhang@hotmail.com (M. Zhang), haoce_dlut@126.com (C. Hao).

http://dx.doi.org/10.1016/j.saa.2017.04.048
1386-1425/

underlying the luminescence of cyclometalated Pt (II) complexes as optical oxygen sensors remains unclear. Experiments are often from the perspective of dynamic quenching to explain the mechanism of oxygen sensing which is based on dynamic collision between molecular oxygen (triplet) and the excited electronic state of luminescent molecules and then producing the luminescent molecule in the ground state and the singlet excited molecular oxygen [36,37]. So a detailed investigation was needed, we focused on exploring the oxygen sensing mechanism from the perspective of static quenching which resulting from complex formation to enrich the theoretical study of oxygen sensing. In this study, DFT and TDDFT methods were used to investigate the oxygen sensing mechanism of cyclometalated platinum complex Lxp1. Frontier molecular orbitals and electronic configuration of the Lxp1 and the Lxp1–$O_2$ complex were calculated to reveal the mechanism of the luminescence procedure. We also explored photophysical processes by calculating the radiative decay and non-radiative decay rate constants of the Lxp1 and the Lxp1–$O_2$ complex. This theoretical study is expected to provide insights into the design of highly efficient cyclometalated Pt(II) materials for oxygen sensing.

## 2. Computation Methodology

All calculations were implemented using the Gaussian 09 software program [38]. Ground-state and excited-state geometric structures for the representative fragment of the Lxp1, molecular oxygen, and the Lxp1–$O_2$ complex were fully optimized using DFT and TDDFT methods, respectively. All optimized geometries were confirmed by frequency calculation. A hybrid exchange–correlation functional using the Coulomb-attenuating method (CAM-B3LYP) was used for all calculations [39]. LANL2DZ was chosen as the basis sets because of relativistic effects that needed to be considered [40,41]. While for excitation energies, we used the LANL2DZ basis sets for the Pt atom and the 6-31G + (d, p) basis sets for other light atoms. In addition, the frontier molecular orbitals and electronic configurations were calculated with the ADF 2012 program, by employing the GGA: PBE functional and the slater-type TZP basis sets [42,43]. The MOMAP package [44–48] was employed to calculate the rate constants of the photophysical processes of the Lxp1 and the Lxp1–$O_2$ complex. The binding energies of hydrogen bonds were calculated using the counterpoise method.

## 3. Results and Discussion

### 3.1. Molecular Geometries in the Ground State

We intercepted a suitable finite representative fragment of the Lxp1 from the periodic structure to simplify computational processes (denoted as motif). Fig. 1(a) presents the geometric configuration of the fragment, which was constructed from 2-phenylpyridine with a fluorophenyl substituent at para position and an acetyl acetone moiety with Pt(II) ions as the node. The optimized geometry parameters (bond lengths, bond angles, and dihedral angles) and the corresponding experimental values [35] of the motif are listed in Table 1. Meanwhile, the calculated UV–vis spectrum with the maximum absorption band at 278 nm is in good agreement with the experimental value 296 nm (Table 1). These deviations were rather small, which indicated that the precision of the calculation was satisfactory and that the CAMB3LYP/LanL2DZ level was suitable for both the structural and electronic features of the motif and the complexes examined. In addition, the structural fragment we used provides a credible representation of the periodic crystal structure system.

The interaction of molecular oxygen with the motif at different sites leads to the formation of different complexes (denoted as complex 1–6), as shown in Fig. 2. Unlike many other molecules, the ground state of oxygen molecule is a spin triplet [49]. This finding was verified by optimizing the oxygen molecule with the CAMB3LYP functional LanL2DZ basis sets in the singlet ($S_0$) and triplet ($T_0$) states, respectively. The energies obtained were −94,253.21 and −94,292.97 kcal/mol. This comparison suggested that the stable equilibrium configuration of oxygen is in $T_0$ state. Similarly, we also optimized the motif in singlet ($S_0$) and triplet ($T_0$) states, with energies of −798,604.07 and −798,543.99 kcal/mol, respectively. We can conclude that the stable conformation of the motif is in $S_0$ state. Therefore, the complexes formed by the motif and the oxygen molecule might have two probabilities of spin multiplicity. We then verified that by calculating the energy of the complexes in $S_0$ and $T_0$ states. We found that the energy of $S_0$ ranged from −892,864.91 kcal/mol to −892,853.75 kcal/mol, whereas the energy of $T_0$ ranged from −892,898.65 kcal/mol to −892,897.97 kcal/mol. Therefore, the complexes with 3 as spin multiplicity had the lower energy. And the ground state of complexes is in $T_0$ states, which is similar to the oxygen molecule. Fig. 2 shows the geometries of complexes with 3 as the spin multiplicity. Intermolecular hydrogen bonds were formed between the motif and the oxygen molecule ranging from 2.46 Å to 2.62 Å. Binding sites with the lowest energy hydrogen-bonded complex 2 for further research to reveal oxygen sensing mechanism. Fig. 1(b) shows the optimized geometric structure of the complex 2. We also calculated the binding energy of the complex 2, which was determined to be −290.26 kJ/mol, fully demonstrating that the relatively strong hydrogen bonding were formed between the motif and the oxygen molecule.

### 3.2. Frontier Molecular Orbitals and Electronic Configuration

The relevant luminescent mechanism of cyclometalated Pt(II) complexes are closely related to the characters of their frontier molecular

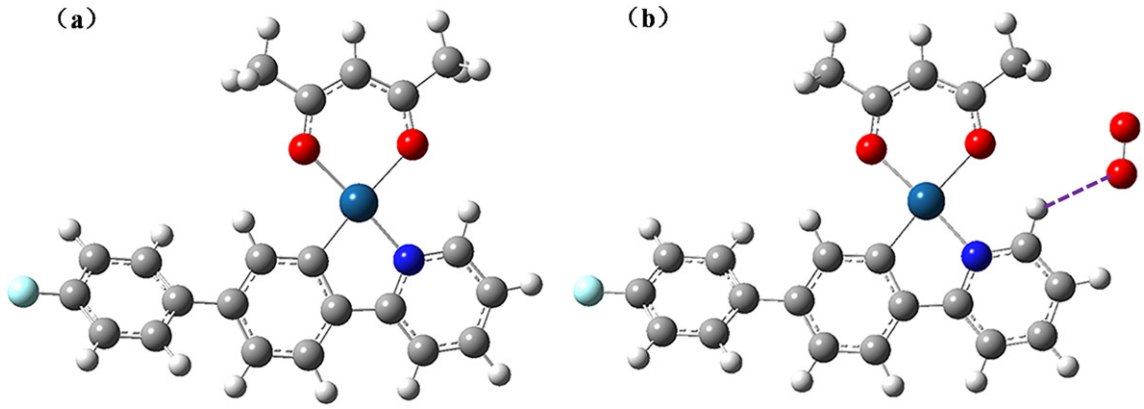


**Fig. 1.** (a) The geometric configuration of structure fragment denoted as motif. (b) Oxygen and motif formed the most stable structure hydrogen bonded complex denoted as complex 2; the purple dotted lines represent the hydrogen bonds (blue represents Pt atom; dark blue represents N atom; red represents O atom; gray represents C atom; white represents H atom; light green represents F atom).

**Table 1**
The geometric configuration, UV–vis spectrum of motif and its corresponding experimental values by (DFT/TDDFT) methods.

| | Cal. values | Exp. values[35] |
|---|---|---|
| *Bond lengths (Å)* | | |
| N42-Pt45 | 2.007 | 1.984 |
| C17-Pt45 | 1.983 | 1.976 |
| O44-Pt45 | 2.116 | 2.073 |
| O43-Pt45 | 2.031 | 1.994 |
| N16-C20 | 1.464 | 1.460 |
| C33-C34 | 1.412 | 1.411 |
| *Bond angles (°)* | | |
| N42-Pt45-C17 | 81.40 | 81.42 |
| O44-Pt45-O43 | 89.93 | 91.70 |
| N42-Pt45-O44 | 94.16 | 94.10 |
| C17-Pt45-O43 | 94.49 | 92.97 |
| *Dihedral angles (°)* | | |
| C20-N42-Pt45-O44 | 179.82 | 178.09 |
| UV–vis maximum absorption (nm) | 278 | 296 |

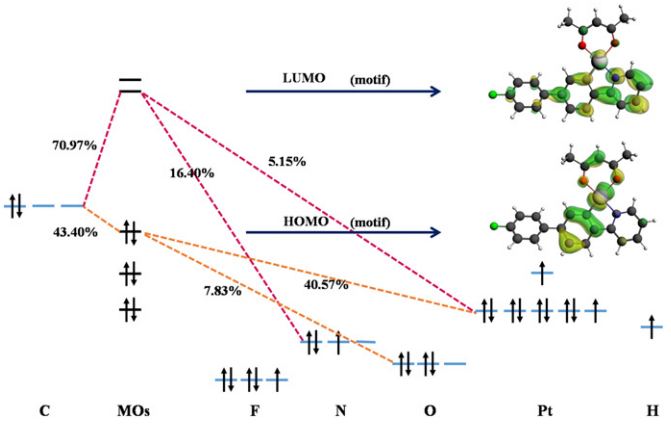


**Fig. 3.** The frontier molecular orbitals and electronic configuration of motif.

orbitals and electronic configuration, particularly their highest occupied molecular orbital (HOMO) and lowest unoccupied molecular orbital (LUMO). Thus, the analysis of the frontier molecular orbitals and electronic configuration of the motif and the complex 2 was carried out using DFT method in this study, as shown in Figs. 3 and 4. It is apparent from Fig. 3 that the electron density distribution of the HOMO primarily resides on the platinum center, the phenyl ring of 2-phenylpyridine, and acetyl acetone moiety. Meanwhile, the LUMO electron density mainly locates on the 2-phenylpyridine ligands. From the electronic configurations of the motif, the HOMO was mainly composed of Pt (3d) (40.57%), C (1p) (43.40%), and N (1P) (1.38%), and O (1P) (7.83%) atoms, whereas the LUMO mainly consisted of Pt (3d) (5.15%), C (1p) (70.97%), and N (1P) (16.40%) atoms. In conclusion, the HOMO has a significant mixture of metal Pt (d) as well as 2-phenylpyridine and acetyl acetone ($\pi$). The LUMO primarily locates on $\pi^*$ of 2-phenylpyridineligands, no obvious interaction between the metal-centered orbitals and the ligand can be observed in the LUMO. Therefore the charge transition involved in the excitation process can be described as [d(Pt) + $\pi$(aac)$\pi^*$(ppy)], where ppy = 2-phenylpyridine, and acac = acetyl acetone. The analysis of the frontier molecular orbitals and electronic configuration led to the conclusion that the luminescence of the motif was assigned to the mixing of ligand-to-metal charge transfer (LMCT) and ligand-to-ligand charge transfer (LLCT) characters. We also analyzed the frontier molecular orbital and the electronic configurations of the complex 2 presented. The ground state of the complex 2 was in $T_0$ state, which had 2 single electrons and therefore had two pairs of HOMO and LUMO orbitals, which were denoted as HOMO-A, HOMO-B, LUMO-A, LUMO-B. As is shown in Fig. 4, that the electron density distribution of HOMO-A of the complex 2 was almost the same with that of the motif, which mainly consisted of the Pt (3d) (39.49%), C (1p) (44.04%), N (1p) (1.39%), and O (1p) (7.55%) atoms. The HOMO-B of complex 2 mainly consisted of the Pt (3d) (38.31%), C (1p) (41.41%), N (1p) (1.37%), and O (1p) (11.89%) atoms. However, the electron density distributions of the LUMO between the complex 2 and the motif had numerous differences. The LUMO-A and the LUMO-B consisted of 94.18% and 98.74% O (1p) atoms, respectively, suggesting that the charge was completely transferred to the oxygen molecule. Therefore the charge transition involved in the excitation process of the complex 2 can be described as [d(Pt) +

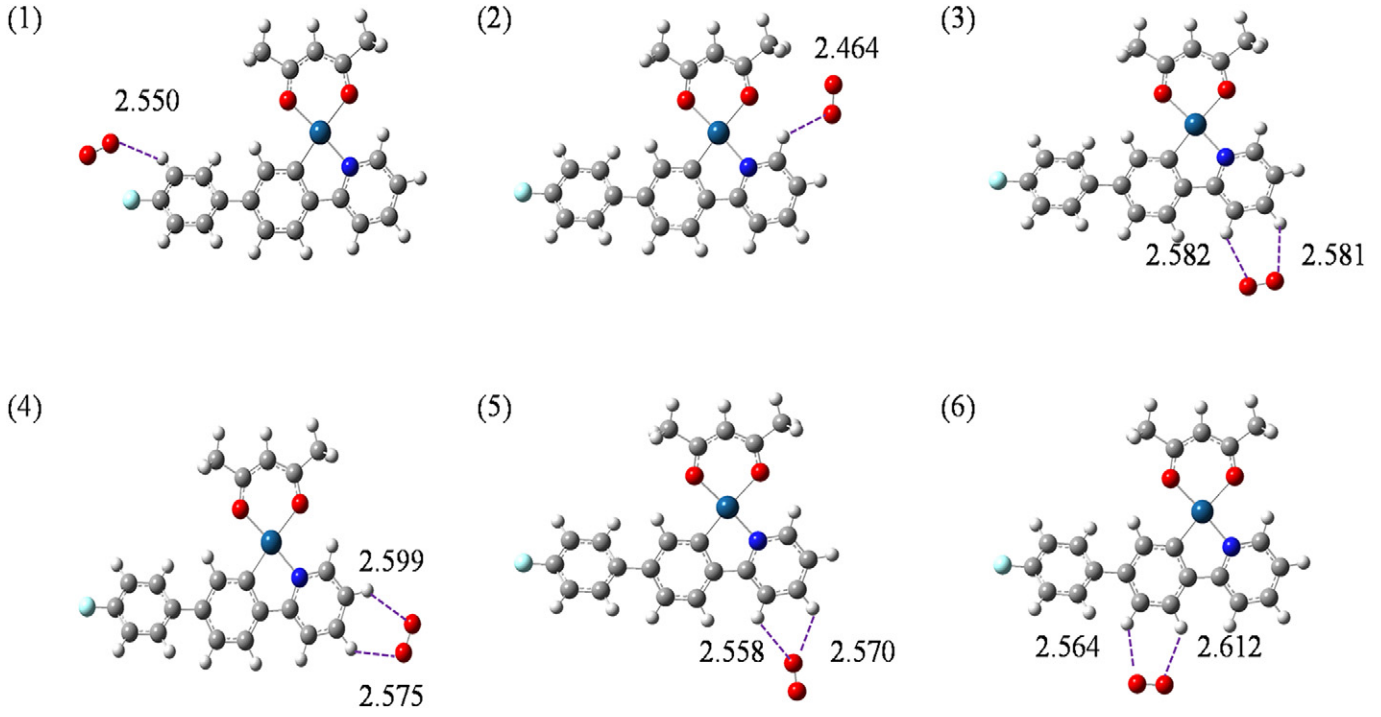


**Fig. 2.** Different possible sites and optimized geometric configurations of complexes 1–6 in $T_0$ state.

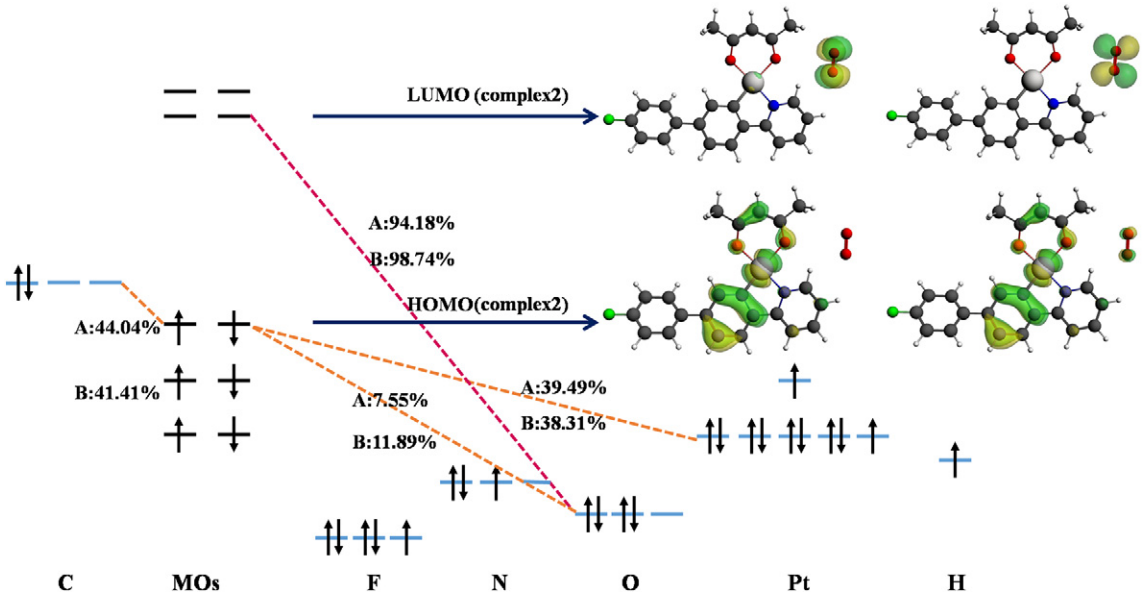


**Fig. 4.** The frontier molecular orbitals and electronic configuration of complex 2.

$\pi$(acac) → $\pi^*$(oxygen)]. And we concluded that the emission of complex 2 could be attributed to the charge transfer from the oxygen molecule to the luminescent material Lxp1. Which indicates that the luminescence mechanism of this system was completely changed after interacting with the oxygen molecule.

### 3.3. Calculated Excitation Energies

Electronic excitation can be significantly influenced by hydrogen bonding, which causes the charge distribution of the hydrogen-bonded complex in different electronic states. To shed light on the nature of hydrogen bonding in this system, we calculated the electronic transition energies of the motif and the complex 2 in the first ten different electronic states on the basis of geometric optimization utilizing TDDFT method. Table 2 shows the results of calculated electronic transition energies and corresponding oscillation strengths of the motif and the complex 2. It can be seen that the electronic transition energies of the complex 2 are lower than those of the motif. According to the rule summarized by Zhao et al. [51], enhanced hydrogen bonding in the excited state could induce a reduction of electronic transition energies, resulting in a red-shift in electronic spectra. Besides, the rule also revealed that the change in electronic excitation energies can predict the behavior of hydrogen bonding in the excited state. The decrease of electronic excitation energy of the complex 2 effectively induces a electronic spectrum red-shift, meanwhile hydrogen bonding in the excited state is strengthened.

For the purpose of exploring the nature of the electronic transitions for different excited states, here we provided the natural transition orbitals (NTOs) of the first three singlet and triplet excitations, respectively. The dominant "particle"–"hole" contributions and the associated weights for the first three singlet ($S_0 \rightarrow S_n$, n = 1, 2 and 3) and triplet ($T_0 \rightarrow T_n$, n = 1, 2 and 3) states of the motif and the complex 2 was obtained in Fig. 5, while the other states ($S_4$ to $S_{10}$ and $T_4$ to $T_{10}$) are plotted in Fig. S1. Particularly, among the ten singlet excited states of the motif, almost all "particle" and "hole" primary reside on the same position, maintain the local exciton character. Which indicate that all the ten singlet excited states of the motif exhibit the LE transition feature. While for the complex 2, among the ten triplet excited states, almost all "particle" mainly locates on the platinum center, the phenyl ring of 2-phenylpyridine, and acetyl acetone moiety. And all "hole" primary resides on the oxygen molecule. Which indicate that almost all the ten triplet excited states of the complex 2 exhibit the CT transition feature. That implying a LE process changed to the CT process upon the electron excitation after interaction with oxygen molecule.

**Table 2**
The electronic excitation energies (eV) and corresponding oscillation strengths of motif and complex 2 by TDDFT method.

| Excited states | Motif | Complex 2 |
|---|---|---|
| $S_1/T_1$ | 3.477 (0.128) | 2.510 (0.000) |
| $S_2/T_2$ | 4.037 (0.011) | 2.905 (0.000) |
| $S_3/T_3$ | 4.063 (0.167) | 3.014 (0.000) |
| $S_4/T_4$ | 4.202 (0.053) | 3.019 (0.002) |
| $S_5/T_5$ | 4.289 (0.028) | 3.244 (0.000) |
| $S_6/T_6$ | 4.454 (0.560) | 3.279 (0.001) |
| $S_7/T_7$ | 4.515 (0.001) | 3.291 (0.000) |
| $S_8/T_8$ | 4.591 (0.041) | 3.317 (0.001) |
| $S_9/T_9$ | 4.593 (0.004) | 3.490 (0.123) |
| $S_{10}/T_{10}$ | 4.711 (0.084) | 3.585 (0.000) |

### 3.4. Photophysical Process of Motif and Complex 2

When the molecule was optically excited, the singlet and triplet electrons could be populated in excited states higher in energy. The electron could then rapidly relax to the lowest excited $S_1$ and $T_1$ states before radiative and non-radiative transitions. Therefore, we only discuss the lowest excited state and ground state. Singlet excisions relax to the ground state via radiative transitions that yield prompt fluorescence, which mainly originates from the dipole-allowed transition between the excited singlet state and the ground state. For internal conversion (IC), the singlet excisions can also relax to the ground state, which is the non-radiative process. Whereas the radiative decay of triplet excitons to the ground state is referred to phosphorescence, which is spin–orbit coupling induced transitions from the excited triplet state to the ground state, but the complexes often experience vertical transition from the ground state to the singlet excited state and then undergo intersystem crossing to reach the triplet excited state in which phosphorescence might occur. The triplet excitons can also relax to the ground state through intersystem crossing (ISC). With Fermi's

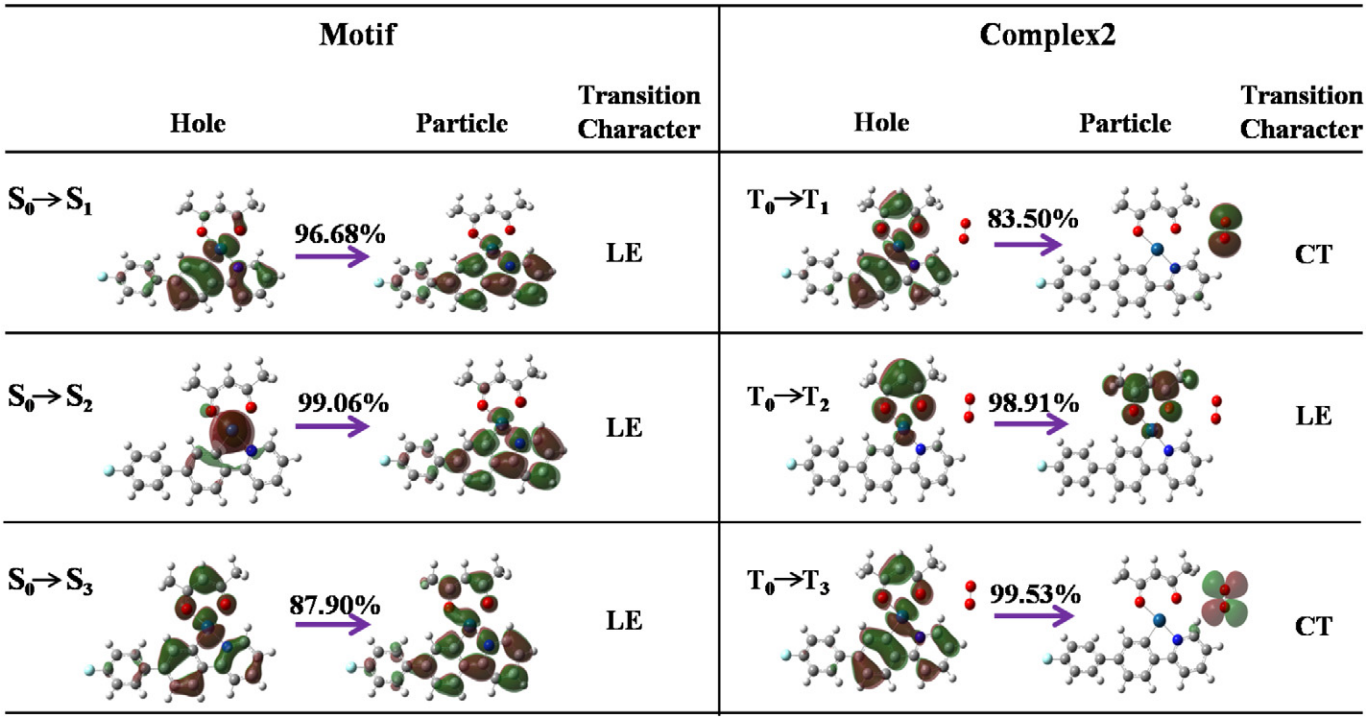


**Fig. 5.** Natural transition orbitals (NTOs) of the first three singlet and triplet excited states for motif and complex 2.

golden rule and time-dependent perturbation theory, all kinds of deactivated rate constant can be obtained by quantum chemistry calculation, including fluorescence ($k_f$), intersystem crossing ($k_{isc}$), internal conversion ($k_{ic}$), and phosphorescence ($k_P$). These processes are presented in the Jablonski diagram in Figs. 6 and 7. The fluorescence radiative decay rate can be expressed as

$$k_f = \frac{64\pi^4}{3hc^3}|u|^2 \sum_a \upsilon_{i0\to fa}{}^3 \left|\int \Theta_{fa} * \Theta_{i0} dQ\right|^2 \quad (2)$$

where $\upsilon_{i0\to fa}$ is the frequency of spontaneous transition from the initial state (usually the first excited state) to the final state (usually the ground state); m is the electric transition dipole moment between the two states; $\Theta_{i0}$ and $\Theta_{fa}$ are the vibrational functions for the initial and final states, respectively, h is the Planck constant; and c is the speed of light in vacuum [44].

The IC rate denoted by $k_{ic}$ [46] can be expressed as

$$k_{ic} = \frac{2\pi}{\hbar}\left|H'_{fi}\right|^2 \delta\left(E_{fi} + E_{f\upsilon_f} - E_{i\upsilon_i}\right) \quad (3)$$

where the perturbation is the non-Born-Oppenheimer coupling

$$H'_{fi} = -\hbar^2 \sum_l \left\langle \Phi_f \Theta_{f\upsilon_f} \left| \frac{\partial \Phi_i}{\partial Q_{fl}} \frac{\partial \Theta_{i\upsilon_i}}{\partial Q_{fl}} \right\rangle \right. \quad (4)$$

Applying the Franck–Condon approximation, the phosphorescence spectrum can be expressed as

$$k_P(\omega, T) = \frac{4\omega}{3\hbar c^3} \sum_{\upsilon_i \upsilon_f} P_{i\upsilon_i}(T) \left|\left\langle \Theta_{f,\upsilon_f} |\mu_{st}| \Theta_{i,\upsilon_i} \right\rangle\right|^2 \delta\left(\omega_{i\upsilon_i, f\upsilon_f} - \omega\right) \quad (5)$$

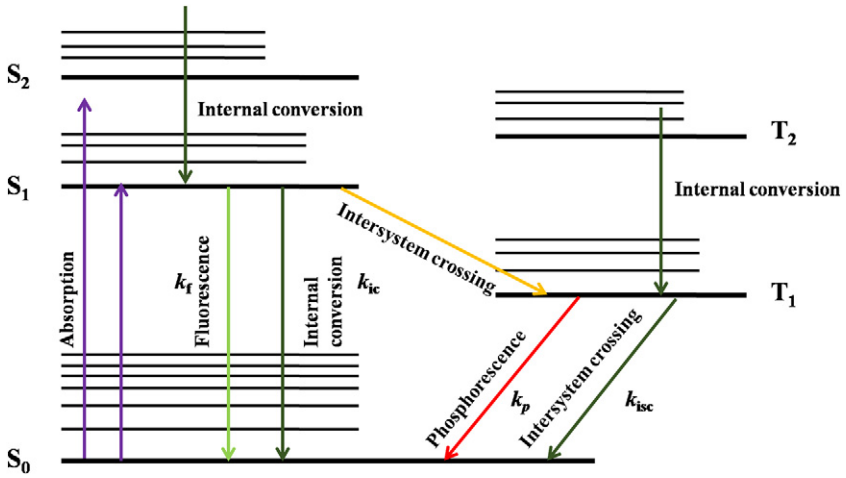


**Fig. 6.** Partial Jablonski diagram for absorption, fluorescence, phosphorescence, internal conversion and intersystem crossing processes of motif.

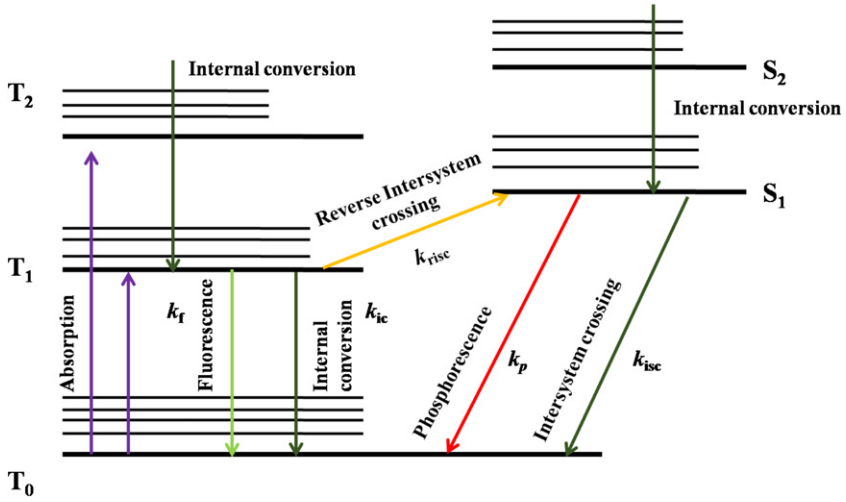


**Fig. 7.** Partial Jablonski diagram for absorption, fluorescence, phosphorescence, internal conversion and intersystem crossing processes of complex 2.

The transition dipole moment can thus be expressed as

$$\boldsymbol{\mu}_{st} = \sum_{k}^{\{\text{singlets}\}} \frac{\langle s|\mu|^1 k\rangle\langle^1 k|\hat{H}^{SO}|T_k\rangle}{^3E_T^0 - {}^1E_k^0} + \sum_{\text{n}}^{\{\text{triplets}\}} \sum_{k'=1}^{3} \frac{\left\langle s\left|\hat{H}^{SO}\right|^3\text{n}_{k'}\right\rangle\langle^3\text{n}_{k'}|\mu|T_k\rangle}{^1E_s^0 - {}^3E_{\text{n}}^0} \quad (6)$$

where $k$ is the magnetic quantum number, n and $k'$ are the intermediate triplet and singlet electronic states, respectively [47].

The intersystem crossing rate constant denoted by $k_{\text{isc}}$ can be expressed as

$$k_{\text{isc}} = \frac{2\pi}{\hbar}\sum_{v_i,v_f} P_{iv_i}\left|\left\langle\Phi_f\Theta_{fv_f}\left|\hat{H}^{SO}\right|\Phi_i\Theta_{iv_i}\right\rangle\right|^2\delta\left(E_{iv_i} - E_{fv_f}\right) \quad (7)$$

where $P_{iv_i}$ is the Boltzmann distribution function for the initial vibronic manifold, H′ denotes the interaction between two different Born–Oppenheimer states, and the delta function δ maintains the conservation of energy.

Applying the Condon approximation,

$$k_{\text{isc}} = \frac{2\pi}{\hbar}R_{\text{fi}}^{\text{isc}}Z_i^{-1}\sum_{v_i,v_f} e^{-\beta E_{iv_i}}\left|\left\langle\Theta_{fv_f}|\Theta_{iv_i}\right\rangle\right|^2\delta\left(E_{iv_i} - E_{fv_f}\right) \quad (8)$$

where $Z_i^{-1} = \sum_{v=\{0_1,0_2,\ldots,0_N\}}^{\infty} e^{-\beta E_v^i}$, $E_v^i$ is the partition function, and $\beta = 1/(k_B T)$. N is the number of normal modes.

$$R_{\text{fi}}^{\text{isc}} \equiv \left|H_{\text{fi}}^{SO}\right|^2 \equiv \left|\left\langle\Phi_f\left|\hat{H}^{SO}\right|\Phi_i\right\rangle\right|^2 \quad (9)$$

is the spin–orbit coupling between the initial and final electronic states. To eclucidate the photophysical process of the motif and complex 2 in detail, we calculated of the radiative decay and non-radiative decay rate constants based on preceding geometry optimizations and vibrational modes for the ground and excited states in Table 3, including the phosphorescence rate constants and the ISC rate constants of the motif, as well as the fluorescent rate constants and the IC rate constants of complex 2. We further analyzed the possible luminescence process of the motif and the complex 2 according to the rate coefficients calculated. We can speculate that the possible luminescence process of the motif is described as follows: the electrons are excited from the ground state to the singlet excited state and then through intersystem crossing falls to the triplet excited state by the heavy-metal effect of Pt atom [50], and then phosphorescence emission would compete with intersystem crossing process from $T_1$-$S_0$. From our calculation, we can find that the phosphorescence rate constant is far greater than the intersystem crossing rate constant, hence a more competitive radiation decay of $T_1 \rightarrow S_0$ than the non-radiation decay of $T_1 \rightarrow S_0$ for the motif, leading to phosphorescence emission of the motif. Meanwhile, the complex 2, which has an unusual triplet ground state, is similar as the oxygen molecule. After being excited, the electrons would jump from the ground state to the triplet excited state. Owing to the existence of Pt atom in the complex 2, reverse intersystem would not occur. Therefore, the deactivation of the excited state would depend on the competition between the fluorescence and IC process. As is shown in Fig. 5, $k_{\text{ic}}$ is much larger then $k_{\text{f}}$, thus, the IC from the excited state to the ground state becomes the most important dissipative process for the complex 2. And finally the oxygen quenching of the cyclometalated Pt(II) complex was observed as mentioned in experiment. By calculating the aforementioned excitation energy, we can conclude that the intermolecular hydrogen bonding was enhanced after the formation of the complex 2. The relationship between the excited state hydrogen bonding dynamics and the IC process was first qualitatively demonstrated by Zhao [51–56]. The deactivation of the excited state via IC can be remarkably facilitated by the intermolecular hydrogen bonding interactions. The IC rate coefficient is significantly larger than the fluorescence rate coefficient we obtained, which is consistent with the theory. The IC process is the main photophysical process contributes to the luminescence quenching phenomenon of complex 2.

**Table 3**
The rate constants of motif and complex 2.

| Rate coefficient | Motif | Rate coefficient | Complex 2 |
|---|---|---|---|
| $k_{\text{P}}$ ($s^{-1}$) | $2.621 \times 10^5$ | $k_{\text{f}}$ ($s^{-1}$) | $6.494 \times 10^1$ |
| $k_{\text{isc}}$ ($s^{-1}$) | $2.410 \times 10^1$ | $k_{\text{ic}}$ ($s^{-1}$) | $1.023 \times 10^7$ |

By analysis of the photophysical processes of the motif and the complex 2, we verified that the motif exhibits phosphorescence emission, as observed in the experiment by DFT and TDDFT methods. We also discovered a new mechanism responsible for luminescence quenching of cyclometalated Pt (II) complexes after interacting with the oxygen molecule. The interaction with oxygen molecule can convert the phosphorescence from $T_1$-$S_0$ of the motif into the IC from $T_1$-$T_0$ of the complex 2. The lifetime of the motif is 3816 ns in our calculation, which has a good agreement with the experiment value 4410 ns [35].

## 4. Conclusions

In this study, we explained the influence of the oxygen molecule on the luminescent properties of the cyclometalated Pt(II) complex and

calculated the geometry optimizations, electronic structures, and photophysical properties of the motif and the complex 2 by DFT/TDDFT methods. Compared with frontier molecular orbitals and electronic configuration, the LUMO changed distinctly after introducing the oxygen molecule. This above mentioned common revealed that the luminescence mechanism of the motif originates from the lowest triplet excited state, which is assigned to the mixing of ligand-to-metal charge transfer and ligand-to-ligand charge transfer character. We also demonstrated that the hydrogen bonding was enhanced in the excited state on the basis of the calculation of electronic excitation energies. The strengthening of Hydrogen bonding in the $T_1$ state would enhance IC, leading to luminescence quenching of cyclometalated Pt(II) complexes after interacting with oxygen molecule. Through the calculation of the rate constants and analysis of the photophysical process of the motif and the complex 2. We confirmed that the motif is a phosphorescent molecule; in addition, molecular oxygen can alter the phosphorescence from $T_1$-$S_0$ to the IC from $T_1$-$T_0$, which indicating that the motif could be used as a chemical sensor for oxygen sensing. The approach employed in our study could be used to understand the mechanism of oxygen sensing and provides a theoretical guidance in the design of different cyclometalated Pt (II) material as oxygen sensors.

## Acknowledgements

This work was supported by NSFC Nos. 21673237 and 21677029.

## Appendix A. Supplementary data

Supplementary data to this article can be found online at http://dx.doi.org/10.1016/j.saa.2017.04.048.

## References

[1] S. Nagl, C. Baleizao, S.M. Borisov, M. Schaferling, M.N. Berberan-Santos, O.S. Wolfbeis, Angew. Chem. Int. Ed. 46 (2007) 2317–2319.
[2] D.A. Skoog, D.M. West, F.J. Holler, Fundamentals of Analytical Chemistry, 1988 344.
[3] R. Ramamoothy, P.K. Dutta, S.A. Akbar, J. Mater. Sci. 38 (2003) 4271–4282.
[4] H.D. Hendricks, US Patent, 3, 1973 663–709.
[5] T.M. Freeman, W.R. Seitz, Anal. Chem. 53 (1981) 98–102.
[6] X.D. Wang, O.S. Wolfbeis, Chem. Soc. Rev. 43 (2014) 3666–3761.
[7] M.M. Suárez, B.F.E. Curchod, I. Tavernelli, U. Rothlisberger, R. Scopelliti, I. Jung, D.D. Censo, M. Gratzel, J.F.F. Sánchez, A.F. Gutiérrez, M.K. Nazeeruddin, E. Baranoff, Chem. Mater. 24 (2012) 2330–2338.
[8] Y. Amao, Microchim. Acta 143 (2003) 1–12.
[9] C. Pulido, O. Esteban, Sensors Actuators B 184 (2013) 64–69.
[10] Y. Amao, K. Asai, I. Okura, Bull. Chem. Soc. Jpn. 72 (1999) 2223–2227.
[11] M. Schferling, Angew. Chem. Int. Ed. 51 (2012) 3532–3554.
[12] C. Baleizao, S. Nagl, M. Schaferling, M.N. Berberan-Santos, O.S. Wolfbeis, Anal. Chem. 80 (2008) 6449–6457.
[13] S. Kochmann, C. Baleizão, M.N. Berberan-Santos, O.S. Wolfbei, Anal. Chem. 85 (2013) 1300–1304.
[14] G.Q. Zhang, G.M. Palmer, M.W. Dewhirst, C.L. Fraser, Nat. Mater. 8 (2009) 747–751.
[15] P. Lehner, C. Staudinger, S.M. Borisov, I. Klimant, Nat. Commun. (2014) 1–6.
[16] C.S. Chu, Y.L. Lo, T.W. Sung, Talanta (2010) 1044–1051.
[17] C.S. Chu, Y.L. Lo, Sensors Actuators B 155 (2011) 53–57.
[18] Q. Zhao, X.B. Zhou, T.Y. Cao, K.Y. Zhang, L.J. Yang, S.J. Liu, H. Liang, H.R. Yang, F.Y. Li, W. Huang, Chem. Sci. 6 (2015) 1825–1831.
[19] A. Mills, A. Lepre, Anal. Chem. 69 (1997) 4653–4659.
[20] C. Liu, X.L. Song, X.F. Rao, Y. Xing, Z.G. Wang, J.Z. Zhao, J.S. Qiu, Dyes Pigments 101 (2014) 85–92.
[21] Y. Amao, T. Miyashita, I. Okura, Analyst 125 (2000) 871–875.
[22] Y. Amao, K. Asai, I. Okura, H. Shinohara, H. Nishide, Analyst 125 (2000) 1911–1914.
[23] C.J. Lin, C.Y. Chen, S.K. Kundu, J.S. Yang, Inorg. Chem. 53 (2014) 737–745.
[24] H.D. Zhang, Y.H. Sun, K.Q. Ye, P. Zhang, Y. Wang, J. Mater. Chem. 15 (2005) 3181–3186.
[25] Y. Amao, Y. Tabuchi, Y. Yamashita, K. Kimura, Eur. Polym. J. 38 (2002) 675–681.
[26] C.S. Chu, C.Y. Chuang, J. Lumin. 154 (2014) 475–478.
[27] D.B. Papkovsky, Sensors Actuators 29 (1995) 213–218.
[28] J.L. Gejo, D. Haigh, G. Orellana, Langmuir 26 (2010) 2144–2150.
[29] Y. Amao, Y.C. Ishikawa, I. Okura, Anal. Chim. Acta 445 (2001) 177–182.
[30] R.N. Gillander, M.C. Tedford, P.J. Crilly, R.T. Bailey, Anal. Chim. Acta 502 (2004) 1–6.
[31] E.A. Sarduy, A. Baidak, G.C. Vougioukalakis, P.E. Keivanidis, J. Phys. Chem. C 118 (2014) 2361–2369.
[32] B.B. Wang, L.M. Zhang, B. Li, Y. Li, Y.H. Shi, T.S. Shi, Sensors Actuators B 190 (2014) 93–100.
[33] O.S. Wolfbeis, J. Mater. Chem. 15 (2005) 2657–2669.
[34] D.B. Papkovskii, A.I. Yaropolov, A.P. Savitskii, J. Olah, V.D. Rumyantseva, A.F. Mironov, Biomed. Sci. 2 (1991) 536–539.
[35] Y. Xing, C. Liu, J.H. Xiu, J.Y. Li, Inorg. Chem. 54 (2015) 7783–7790.
[36] X.C. Sun, Y. Wang, Y. Lei, Chem. Soc. Rev. 44 (2015) 8019–8061.
[37] Z.S. Dou, J.C. Yu, Y.J. Cui, Y. Yang, Z.Y. Wang, D. Yang, G.D. Qian, J. Am. Chem. Soc. 136 (2014) 5527–5530.
[38] M.J. Frisch, G.W. Trucks, H.B. Schlegel, G.E. Scuseria, M.A. Robb, J.R. Cheeseman, G. Scalmani, V. Barone, B. Mennucci, G.A. Petersson, H. Nakatsuji, M. Caricato, X. Li, H.P. Hratchian, A.F. Izmaylov, J. Bloino, G. Zheng, J.L. Sonnenberg, M. Hada, M. Ehara, K. Toyota, R. Fukuda, J. Hasegawa, M. Ishida, T. Nakajima, Y. Honda, O. Kitao, H. Nakai, T. Vreven, J.A. Montgomery Jr., J.E. Peralta, F. Ogliaro, M. Bearpark, J.J. Heyd, E. Brothers, K.N. Kudin, V.N. Staroverov, R. Kobayashi, J. Normand, K. Raghavachari, A. Rendell, J.C. Burant, S.S. Iyengar, J. Tomasi, M. Cossi, N. Rega, J.M. Millam, M. Klene, J.E. Knox, J.B. Cross, V. Bakken, C. Adamo, J. Jaramillo, R. Gomperts, R.E. Stratmann, O. Yazyev, A.J. Austin, R. Cammi, C. Pomelli, J.W. Ochterski, R.L. Martin, K. Morokuma, V.G. Zakrzewski, G.A. Voth, P. Salvador, J.J. Dannenberg, S. Dapprich, A.D. Daniels, O. Farkas, J.B. Foresman, J.V. Ortiz, J. Cioslowski, D.J. Fox, Gaussian 09, Revision A. 01, Gaussian, Wallingford, CT, 2009.
[39] T. Yanai, D.P. Tew, N.C. Handy, Chem. Phys. Lett. 393 (2004) 51–57.
[40] P.J. Hay, W.R. Wadt, J. Chem. Phys. 82 (1985) 299–310.
[41] X. Gu, T. Fei, H.Y. Zhang, H. Xu, B. Yang, Y.G. MA, X.D. Liu, J. Phys. Chem. A 112 (2008) 8387–8393.
[42] G. Te Velde, F.M. Bickelhaupt, S.J.A. Van Gisbergen, C. Fonseca Guerra, E.J. Baerends, J.G. Snijders, T. Ziegler, J. Comput. Chem. 22 (2001) 931–967.
[43] C.F. Guerra, J.G. Snijders, G. Te Velde, E.J. Baerends, Theor. Chem. Accounts 99 (1998) 391–403.
[44] Q. Peng, Y.P. Yi, Z.G. Shuai, J.S. Shao, J. Am. Chem. Soc. 129 (2007) 9333–9339.
[45] Y.L. Niu, Q. Peng, C.M. Deng, X. Gao, Z.G. Shuai, J. Phys. Chem. A 114 (2010) 7817–7831.
[46] Y.L. Niu, Q. Peng, Z.G. Shuai, Sci. China, Ser. B: Chem. 51 (2008) 1153–1158.
[47] Z.G. Shuai, Q. Peng, Phys. Rep. 537 (2014) 123–156.
[48] Q. Peng, Y.L. Niu, Q.H. Shi, J. Chem. Theory Comput. 9 (2013) 1132–1143.
[49] Y. Feng, J.H. Cheng, L. Zhou, X.G. Zhou, H.F. Xiang, Analyst 137 (2012) 4885–4901.
[50] B. Minaev, X. Li, Z.J. Ning, H. Tian, H. Agren, Organic Light Emitting Diode - Material, Process and Device [M], 2011 62–100.
[51] G.J. Zhao, K.L. Han, Acc. Chem. Res. 45 (2012) 404.
[52] C.L. Cheng, G.J. Zhao, Nano 4 (2012) 2301.
[53] G.J. Zhao, J.Y. Liu, L.C. Zhou, K.L. Han, J. Phys. Chem. B 111 (2007) 8940–8945.
[54] M.X. Zhang, G.J. Zhao, ChemSusChem 5 (2012) 879.
[55] G.J. Zhao, K.L. Han, J. Phys. Chem. A 111 (2007) 2469.
[56] G.J. Zhao, K.L. Han, ChemPhysChem 9 (2008) 1842–1846.